PROCEEDINGS OF SCIENCE

Exclusive hadronic cross sections measured via ISR from *BABAR*

Andreas Hafner*
Institut für Kernphysik, Johannes Gutenberg Universität Mainz,
J.-J.-Becher-Weg 45, 55099 Mainz, Deutschland.
E-mail: hafner@slac.stanford.edu

Measuring the inclusive hadronic cross section in e^+e^- annihilation is of major interest for the determination of the Standard Model prediction of the anomalous magnetic moment of the muon a_μ. The QED and weak contribution to a_μ can be calculated with very high precission. At low energies, however, perturbation theory cannot be used to calculate the hadronic contribution $a_\mu^{\rm had}$. It therefore has to be derived via a dispersion relation from the sum of measured cross sections of exclusive hadronic reactions. Decreasing the experimental uncertainties on these channels is of utmost importance for an improved Standard Model prediction of a_μ. Between 1999 and 2008 a data sample corresponding to an integrated luminosity of approximately 500 fb^{-1} was recorded with the *BABAR* detector at the PEP-II asymmetric-energy e^+e^- collider at SLAC operating at and near center-of-mass energy 10.58 GeV. Using events produced via Initial State Radiation the energy range from threshold up to 4.5 GeV can be accessed. Cross section measurements for the processes $e^+e^- \to h_1^+h_1^-h_2^+h_2^-$ ($h_{1/2} = \pi$ or K) and $e^+e^- \to K^+K^-\pi^0\pi^0$ are presented.

36th International Conference on High Energy Physics,
July 4-11, 2012
Melbourne, Australia

*Speaker.

PoS(ICHEP2012)276

1. Introduction

The particular interest in hadronic cross section measurements arises due to the discrepancy between the value of the anomalous magnetic moment of the muon $a_\mu = \frac{1}{2}(g-2)_\mu$ obtained by the E821 experiment at BNL [1] and the prediction from the Standard Model [2]. The QED and weak contributions to a_μ can be calculated with very high precission. At low energies perturbation theory cannot be used to calculate the hadronic contribution $a_\mu^{\rm had}$. However, it is possible to relate the hadronic contribution to the muon anomaly $a_\mu^{\rm had}$ via a dispersion relation to hadronic cross sections, which typically are measured in e^+e^- energy scan experiments at low energies. The study of the Initial State Radiation (ISR) events at B-factories allows independent measurements of these exclusive hadronic cross sections. This method allows high statistics e^+e^- experiments running at a fixed center-of-mass (c.m.) energy to access processes at lower effective c.m. energies by studying events with a high energy photon emitted from the initial state. The use of this technique at high luminosity ϕ- and B-factories has been discussed in detail in Refs. [4, 5, 6]. The *BABAR* Collaboration has an extensive program to investigate low multiplicity ISR processes [7] at effective c.m. energies below 5 GeV. In addition to the cross section measurements, these studies include many additional physics topics, e.g. spectroscopy and form-factor measurements.

The ISR cross section for a particular final state f depends on the non-radiative cross section $\sigma_f(s)$, and is obtained from Eq. (1.1):

$$\frac{d\sigma_{f,\gamma}(m)}{dm} = \frac{2m}{s} \cdot W(s,x,\theta_\gamma^*) \cdot \sigma_f(m), \tag{1.1}$$

where $x = \frac{2 \cdot E_\gamma^*}{\sqrt{s}}$ and $\sqrt{s}$ is the nominal c.m. energy; θ_γ^*, E_γ^*, and W are the polar angle, energy, and the radiation probability of the ISR photon in the nominal c.m. frame, whereby the effective c.m. energy is decreased to $\sqrt{s'} = m$.

Figure 1 shows the distribution of contributions (left) and uncertainties (right) in % for $a_\mu^{\rm had}$ from different energy regions [8]. The low energy contributions are of high importance, e.g. the process $e^+e^- \to \pi^+\pi^-$ contributes with approximately 73% to $a_\mu^{\rm had}$. Due to the very precise measurement of the leading contribution to $a_\mu^{\rm had}$, the leading contribution to the uncertainty stems from the region between 1 GeV and 2 GeV. The four-pion channels are the most significant in this region of interest. The results of the $\pi^+\pi^-\pi^+\pi^-$ analysis are presented here. The measurement of $e^+e^- \to \pi^+\pi^-\pi^0\pi^0$ is still preliminary, but will be finalised and published soon. We also present results for the channels $e^+e^- \to K^+K^-\pi\pi$ with charged and neutral pions, and for $e^+e^- \to K^+K^-K^+K^-$.

2. The *BABAR* experiment

The Stanford Linear Accelerator (SLAC) provided 9 GeV electrons and 3.1 GeV positrons to the asymmetric-energy PEP-II e^+e^- collider. This corresponds to a c.m. energy of $\sqrt{s} = 10.58$ GeV. The *BABAR* detector is described elsewhere [9]. The reconstruction of charged-particle tracks is performed in the tracking system, which comprises a five-layer silicon vertex tracker (SVT) and a 40-layer drift chamber (DCH) in a 1.5 T axial magnetic field. Separation of charged pions, kaons, and protons is achieved with a combination of Cherenkov-angle measurements in the detector

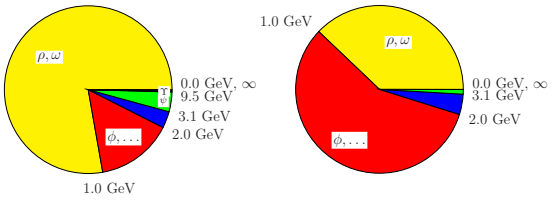

Figure 1: The distribution of contributions (left) and uncertainties (right) in % for $a_\mu^{\rm had}$ from different energy regions [8]. The error of a contribution i shown is $\sigma^2_{itot}/\Sigma_i\sigma^2_{itot}$ in %. The total error combines statistical and systematic errors in quadrature.

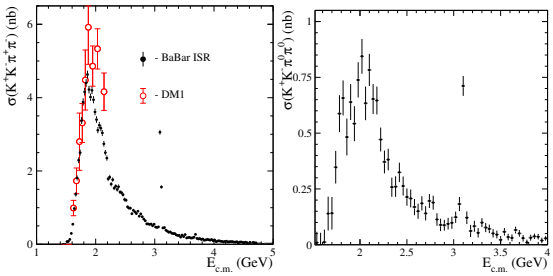

Figure 2: Cross section for the process $e^+e^- \to K^+K^-\pi^+\pi^-$ (left) and $e^+e^- \to K^+K^-\pi^0\pi^0$ (right) for the entire energy range. Only statistical errors are indicated.

of internally reflected Cherenkov light (DIRC) and specific ionization measurements in the SVT and DCH. The CsI(Tl) electromagnetic calorimeter (EMC) measures the energy of photons and electrons. Muon identification is provided by the instrumented flux return (IFR).

A simulation package developed for radiative processes, AfkQed, is used to study the detector acceptance and efficiency. The simulation of hadronic final states is based on an approach suggested by Czyż and Kühn [10]. Additional ISR photons are generated with the structure function method [11], and additional FSR photons with PHOTOS [12]. The ISR background channels simulated with AfkQed have been studied, as have non-radiative continuum background events from $e^+e^- \to q\overline{q}$ ($q = u,d,s,c$), generated with JETSET [13]. The response of the *BABAR* detector is simulated with Geant4 [14]. The generated events are subjected to detector simulation, and are reconstructed with the same software chain used for experimental data events. The detection efficiency obtained by simulation is then corrected by extensive studies of differences between data and MC. Separate studies have been performed in order to determine the tracking and particle identification efficiencies.

The data used in the following analyses correspond to a total integrated luminosity of 454 fb^{-1}. In standard *BABAR* ISR analyses, the high energy photons are detected at large angles with respect to the e^+e^- collision axis. In Fig. 2, the cross section for the channel $K^+K^-\pi\pi$ is shown for charged (left) and neutral (right) pions in the final state. The systematic uncertainty in the peak region is 4%(5%) increasing to 11%(16%) towards higher c.m. energies for the channel with the charged (neutral) pions. In addition to these cross section measurements, the internal structure of these final states is of interest. In Fig. 3(a) the $K^+\pi^-$ invariant mass is plotted versus the $K^-\pi^+$ invariant mass. The plot reveals the presence of the $K^*(892)$, and thus the dominance of the $K^*(892)K^\pm\pi^\mp$ in this final state. The corresponding 1-dimensional projection in Fig. 3(b) shows the presence of the $K_2^*(1430)$ resonance. Selecting the $K^*(892)$ and combining this resonance with another $K^\pm$ or $\pi^\pm$ leads to the scatterplot in Fig. 3(c). Two horizontal bands are visible. The $K^*(892)\pi^\pm$ invariant mass projection (Fig. 3(d)), shows the presence of the $K_1(1270)$ and $K_1(1400)$ resonances. A very clean selection can be performed by requiring that the K^+K^- are the decay products of the narrow $\phi(1020)$ resonance. This selection of $\phi\pi^+\pi^-$ events has a contribution of approximately 10%. The corresponding cross section is shown in Fig. 4(a). The red curve represents a fit based on a model including the $\phi(1680)$ and the Y(2175) resonances. In Fig. 4(b) the $\pi^+\pi^-$ invariant mass distribution is shown. An angular analysis shows that these events are produced in an S-wave state. The two peaking structures are denoted as the $f_0(600)$ and the $f_0(980)$. Selecting only the $f_0(600)$

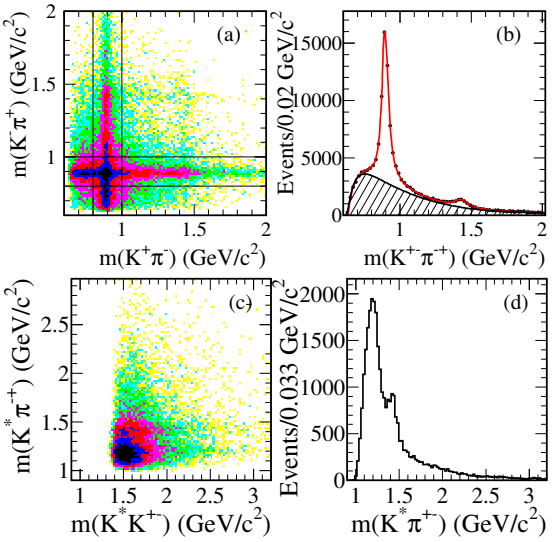

Figure 3: (a) $K^+\pi^-$ vs. $K^-\pi^+$ invariant mass scatterplot, and (b) the corresponding projection. (c) $K^*\pi^\mp$ vs. $K^*K^\mp$ invariant mass scatterplot, and (d) the $K^*\pi^\mp$-projection.

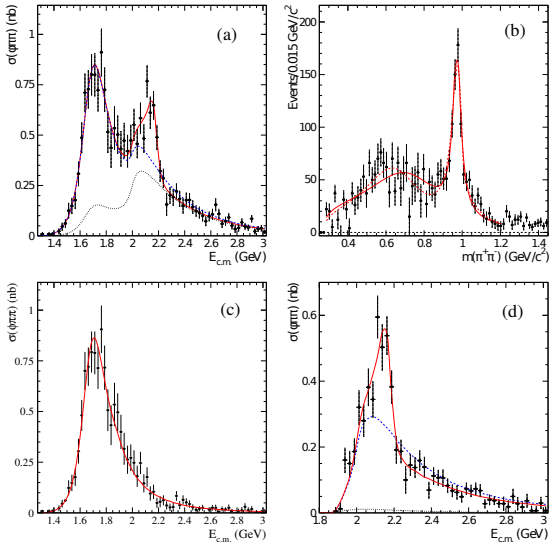

Figure 4: (a) Cross section for $e^+e^- \to \phi\pi^+\pi^-$, (b) the corresponding $\pi^+\pi^-$ invariant mass distribution. (c) Cross section requiring $m(\pi^+\pi^-) < 0.85\,\mathrm{GeV}/c^2$, and (d) $0.85\,\mathrm{GeV}/c^2 < m(\pi^+\pi^-) < 1.1\,\mathrm{GeV}/c^2$. For fit details, see Ref. [7].

events, the cross section for $\phi\pi^+\pi^-$ is plotted in Fig. 4(c). Only the contribution of the $\phi(1680)$ is noticable. Figure 4(d) shows the corresponding distribution for events containing the $f_0(980)$. Here a contribution of the Y(2175) in addition to the $\phi(1680)$ resonance is needed in order to properly describe the observed distribution. Thus, the Y(2175) decays exclusively via the $\phi(1020)f_0(980)$ final state, whereas the $\phi(1680)$ decays additionaly via $\phi(1020)f_0(600)$.

In Fig. 5(a), the cross section for the channel $K^+K^-K^+K^-$ is shown. The J/ψ peak is clearly visible and an additional structure near 2.25 GeV seems to be present. The K^+K^- invariant mass is displayed in Fig. 5(b) as the open histogram (two entries per event). A very strong $\phi(1020)$ contribution is visible. The hatched histogram shows the K^+K^- mass which is closer to the $\phi(1020)$ mass-peak. Thus, there is almost always one $\phi(1020)$ present per event. Restricting one K^+K^- mass combination to the mass region of the $\phi(1020)$ resonance, the invariant mass of the other K^+K^- mass combination is plotted in Fig. 5(c). This region is subdivided into contributions from the $f_0(980)$ (region 1), an unknown contribution (region 2), and the $f_2'(1525)$ (region 3). Figure 5(d) shows the cross section for events from region 1. A signal for the Y(2175) resonance is visible. The cross section for events from region 2 (Fig. 5(e)), is responsible for the structure near 2.25 GeV. Finally region 3, displayed in Fig. 5(f), shows a very strong contribution from the J/ψ resonance.

Concerning the $\pi^+\pi^-\pi^+\pi^-$ final state, the cross section is shown in Fig. 6. The systematic uncertainty of this measurement is 2.4% in the peak region, increasing to 10.7% in the low energy region shown in the inlay, and to 5.5% (8.5%) for energies above 2.8 GeV (4.0 GeV).

The contribution to a_μ^{had} from $e^+e^- \to \pi^+\pi^-\pi^+\pi^-$ based solely on the *BABAR* measurement is estimated to be $a_\mu^{had}(\pi^+\pi^-\pi^+\pi^-) = 13.35 \pm 0.10_{stat} \pm 0.52_{syst}$. This reduces the estimated uncertainty without the *BABAR* data by approximately a factor of 3. This final state also contains various intermediate resonances. The $\pi^+\pi^-\pi^\pm$ invariant mass distribution is shown in the leftmost

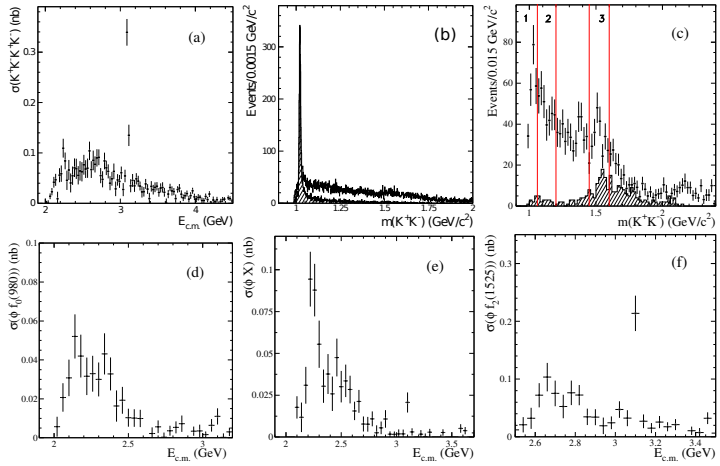

Figure 5: (a) The $e^+e^- \to K^+K^-K^+K^-$ cross section, (b) m(K^+K^-) combination (closer to m(ϕ)) in the open (hatched) histogram, (c) the combination outside the ϕ region. The cross section for (d) region 1, (e) region 2, and (f) region 3 as indicated in (c).

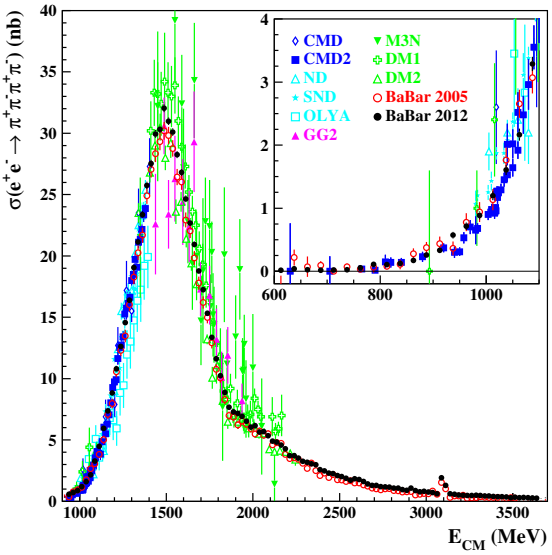

Figure 6: Cross section for the process $e^+e^- \to \pi^+\pi^-\pi^+\pi^-$ measured by different experiments for the entire energy range. Only statistical errors are shown.

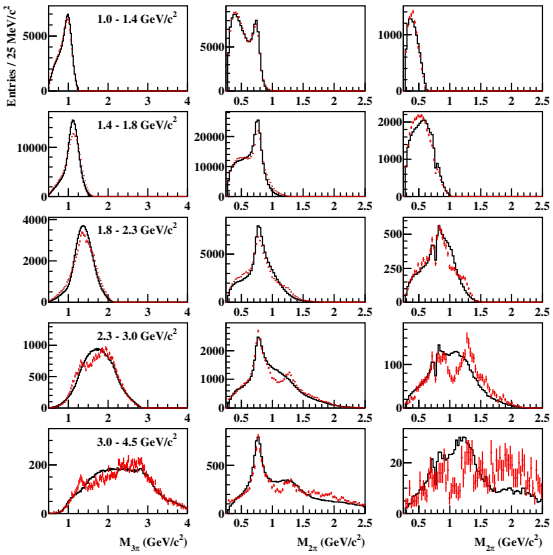

Figure 7: Left: invariant $\pi^+\pi^-\pi^\pm$ mass distributions (4 entries per event) for different regions of $M_{4\pi}$ for the data without background subtraction (points) and signal simulation (histogram); Middle: $\pi^+\pi^-$ mass distributions (4 entries per event); Right: the $\pi^+\pi^-$ mass distribution with the other $\pi^+\pi^-$ mass in the $\rho(770)^0$ mass region.

column of Fig. 7 for different regions of 4π mass. In the low mass region, $1.0 < M_{4\pi} < 1.4\,\mathrm{GeV}/c^2$, there is not enough energy to allow production of the $a_1(1260)^\pm$. At higher $M_{4\pi}$, the contribution of the $a_1(1260)^\pm$ becomes visible. It is observed as a peaking structure with mass and width $M_{3\pi} \approx 1300\,\mathrm{MeV}/c^2$ and $\Gamma \approx 200\,\mathrm{MeV}$, respectively. In the $\pi^+\pi^-$ invariant mass distributions shown in the middle column of Fig. 7, four entries are present per event. At low 4π mass and in the peak region only a single resonance, the $\rho(770)^0$, is observed. At larger 4π mass, a second peaking structure appears at $M_{2\pi} \approx 1270\,\mathrm{MeV}/c^2$, which most likely corresponds to the $f_2(1270)$. Approximately 25% of the entries are in the $\rho(770)^0$ peak. The production of $\rho(770)^0\rho(770)^0$ via

a single virtual photon is not allowed due to C-parity conservation (but see Ref. [15]), leading to the conclusion that in each event one $\rho(770)^0$ meson is present. To investigate the possible presence of the $f_2(1270)\rho(770)^0$ final state, the $\pi^+\pi^-$ combination is plotted for the case that there is another $\pi^+\pi^-$ combination within $\pm 25\,\mathrm{MeV}/c^2$ of the $\rho(770)^0$ mass (Fig. 7, right column). The $f_2(1270)$ resonance is visible as a shoulder in the $1.8 < M_{4\pi} < 2.3\,\mathrm{GeV}/c^2$ mass region. It is even more prominent in the $2.3 < M_{4\pi} < 4.5\,\mathrm{GeV}/c^2$ region, where the energy is large enough to allow direct production of $f_2(1270)\rho(770)^0$. A sharp falloff in the $M_{2\pi}$ spectrum just below $1\,\mathrm{GeV}/c^2$ is visible in the $1.8 < M_{4\pi} < 2.3\,\mathrm{GeV}/c^2$ region. This might be due to interference with the $f_0(980)$ final state. A partial wave analysis would be necessary to determine the amplitude structure of the individual intermediate states.

3. Conclusions

ISR physics is a very productive field in addition to B-physics at *BABAR*. Many measurements were performed or are still ongoing for the first time with high accuracy. These results have an important impact for the theoretical prediction of a_μ. Including hadronic cross section measurements from other experiments the remaining difference between theoretical prediction and measured value of 3-3.5σ [16, 17] for the muon anomaly still poses an open question and requires further studies.

References

[1] G.W.Bennett *et al.* (Muon g-2 Collaboration), Phys. Rev. D **73**, 072003 (2006).

[2] M. Davier (Orsay, LAL), S. Eidelman (Novosibirsk, IYF), A. Hocker, Z. Zhang (Orsay, LAL). LAL-03-50, Aug 2003. 14pp., Eur.Phys.J.C31:503-510,2003 e-Print Archive: hep-ex/0308213

[3] S.J. Brodsky and E. de Rafael, Phys. Rev. **168**, 1620 (1968).

[4] A.B. Arbuzov *et al.*, JHEP **9812**, 009 (1998).

[5] S. Binner, J.H. Kühn, K. Melnikov, Phys. Lett. B **459**, 279 (1999).

[6] M. Benayoun *et al.*, Mod. Phys. Lett. A **14**, 2605 (1999).

[7] B. Aubert *et al.* (*BABAR* Collaboration), PRD **70**, 072004 (2004) , PRD **71**, 052001 (2005) , PRD **73**, 052003 (2006) , PRD **73**, 012005 (2006) , PRD **76**, 092006 (2007) , PRD **76**, 092005 (2007) , PRD **76**, 012008 (2007) , PRD **77**, 092002 (2008) , PRL **103**, 231801 (2009).

[8] F. Jegerlehner and A. Nyffeler, Phys.Rept. **477**, 1 (2009).

[9] B. Aubert *et al.* (*BABAR* Collaboration), Nucl.Instr.Meth. PR A **479**,1 (2002).

[10] H. Czyż and J.H. Kühn, Eur.Phys.J C **18**, 497 (2000).

[11] M. Caffo, H. Czyż, E. Remiddi, Nuo. Cim. A **110**, 515 (1997); Phys. Lett. B **327**, 369 (1994).

[12] E. Barberio, B. van Eijk and Z. Was. Comput. Phys. Commun. **66**, 115 (1991).

[13] T. Sjöstrand, Comput. Phys. Commun. **82**, 74 (1994).

[14] S. Agostinelli *et al.* (Geant4 Collab.), Nucl. Instrum. Methods Phys. Res., Sect. A **506**, 250 (2003).

[15] B.Aubert et *et al.* (*BABAR* Collaboration), PRL **97**, 112002 (2006).

[16] T. Teubner, K. Hagiwara, R. Liao, A.D. Martin, D. Nomura, Nucl.Phys.Proc.Suppl. **218**, 225 (2011).

[17] M. Davier *et al.*, Europ. Phys. J. C **71**, 1515 (2011).